# MAGNETIC RESONANCE IMAGING CHARACTERISATION OF THE INFLUENCE OF FLOWRATE ON LIQUID DISTRIBUTION IN DRIP IRRIGATED HEAP LEACHING


**Authors**

Marijke A. Fagan-Endres [a, b *]

marijke.fagan-endres@uct.ac.za

Susan T.L. Harrison [b]

sue.harrison@uct.ac.za

Michael L. Johns [c]

michael.johns@uwa.edu.au

Andrew J. Sederman [a]

ajs40@cam.ac.uk

[a] Department of Chemical Engineering and Biotechnology, University of Cambridge, Pembroke Street, Cambridge, CB2 3RA, UK

Tel: +44 1223 766338

[b] Centre for Bioprocess Engineering Research, Department of Chemical Engineering, University of Cape Town, Rondebosch, 7701, South Africa

Tel: +27 21 6505522

[c] School of Mechanical and Chemical Engineering, University of Western Australia, 35 Stirling Highway, Crawley, WA 6009, Australia

* Corresponding author

## ABSTRACT

Liquid irrigation is one of the key process control parameters following the construction of an ore leaching heap. This study uses 3D magnetic resonance imaging (MRI) to examine non-invasively the effect of liquid flowrate changes on heap hydrology when drip irrigation is used. Experimental results from a vertical column show that the increase in flowrate causes an increase in the number of rivulets in the ore bed. The new rivulets were found to be thicker, and their development caused an increase in liquid-solid contacting area which is considered advantageous for metal ion recovery. Experiments performed on larger samples showed that the effects of flowrate changes were limited to the region directly below the drip emitter because the increase in flowrate caused an increase in macro-pore flow and not capillary retention of liquid. Therefore the increase in flowrate was not found to perturb liquid distribution patterns in a way that would be substantially advantageous to heap leaching recoveries.

**Keywords**

MRI, Heap leaching, Hydrometallurgy, Flowrate, Interfacial area, Irrigation

# 1 INTRODUCTION

Heap leaching is a (bio)hydrometallurgical extraction technique that is commonly used for the recovery of copper from low grade ores and for the pre-treatment of gold ores to oxidise metal sulphides (e.g. iron and arsenic) prior to cyanidation. The ore to be processed is crushed and typically agglomerated to improve the particle homogeneity before it is packed into large heaps which may be hundreds of metres in length and breadth and up to 20 m in height. In operation the heaps are unsaturated systems which are irrigated from the top with an acidic leaching solution and aerated from the base to supply sufficient oxygen for the leaching reactions and, in the case of bioleaching, carbon dioxide for microorganisms in the heap to fix as biomass. It is in the liquid/solid interphase that the leaching reactions occur, thus contacting of the ore with the liquid is essential to metal recovery. The leaching solution flows downwards through the ore bed under gravity and is collected at the base at which stage it is termed the pregnant leach solution (PLS). The liberated metal ions are transported out of the heap by this flowing liquid, hence the relative distribution of the flowing and stagnant liquid hold-up has a substantial influence on the efficiency of the process. The liquid phase holds further importance in bioleaching operations because it is where the sulfur- and iron-oxidising microorganisms populate.

The liquid feed application is one of the only process control parameters following the construction of the heap. Consequently it is desirable to understand the effect of flowrate changes on the liquid distribution. Heaps are typically irrigated via drip emitters spaced in a 0.5 to 1 m grid-structure and the applied liquid fluxes range between 4 and 18 L $m^{-2}$ $h^{-1}$ (Petersen and Dixon, 2007). Flowrates that are too high can cause short circuiting of the liquid and flooding which deprives the system of oxygen. It can also result in a dilute PLS thereby increasing the difficulty and cost of recovery. On the other hand, flowrates that are

too low can result in excessively long leaching times and in extreme cases the heap may dry out. The flowrate also affects the microbial populations in biological heap leaching systems with Chiume et al. (2012) having demonstrated that faster colonisation of the ore in laboratory columns occurs at lower flowrates, attributed to the reduced detachment of cells and a potential response to nutrient concentration and the degree of oxygen saturation of the liquid.

The choice of flowrate is further complicated by the inhomogeneity of the ore particles and the overall heap structure coupled with the complex nature of unsaturated fluid flow. Liquid distribution in heaps occurs via two mechanisms: gravitational flow downwards through the heap in larger channels and dispersion of the liquid under capillary forces. Capillary distribution of the liquid is the slower of the two and largely accounts for lateral movement of the liquid. This can result in poor wetting of heaps overall, with preferential flow channels forming in the regions below the drip emitters and poor recovery of the desired metals being achieved in the remaining regions (O'Kane Consultants Inc., 2000; Petersen and Dixon, 2003; van Hille et al., 2010). This is well demonstrated in the photographs of a heap cross-section in Petersen and Dixon (2003) which shows clear evidence of solution channels below the drip emitters.

Optimisation of heap irrigation has been approached through a number of studies aimed at improving the understanding of heap hydrodynamics. Direct comparison of heap wetting with trickle bed reactors, as are commonly applied in chemical engineering processes, is not possible due to the comparatively slower flows used in heap leaching (Bouffard and Dixon, 2001). Some success has been had in relating heap hydrodynamics to unsaturated soil theory, based on Darcy's law, specifically with respect to describing how flowrate relates to

preferential flow through regions of different particle sizes (Bartlett, 1998; Decker and Tyler, 1999; O'Kane Consultants Inc., 2000; Wu et al., 2007). Gravimetric and tracer studies have also aided the design and validation of mathematical models to describe heap performance (Bouffard and Dixon, 2001; Bouffard and West-Sells, 2009; De Andrade Lima, 2006; Ilankoon and Neethling, 2012). However a limitation of these studies is that they are all 'black-box' techniques which only allow for approximations of the heap hydrodynamics. Furthermore, laboratory scale studies tend to underestimate the degree of inhomogeneity that is present at full scale operation. This is highlighted by the industrial scale investigations by Guzman et al. (2006) that used Electric Resistivity Tomography (ERT) to measure moisture content throughout a series of heaps. They reported pronounced heterogeneous solution distribution in the heaps and found that this significantly impacted the metal recovery rate and the uniformity of extraction and concluded that the core issue in sulfide leaching in reagent delivery rather than leaching kinetics.

We have shown in a previous study that maps of the liquid distribution in representative leaching systems can be acquired using a specialist magnetic resonance imaging (MRI) technique called spin echo single point imaging (SESPI) which is immune to the detrimental influence of para- and ferromagnetic species in the ore (Fagan et al., 2013; Fagan et al., 2012) and is able to detect liquid both external and internal to the ore. This technique may be used to determine the liquid distribution and position relative to the solid ore and through analysis of temporal changes in signal magnitude, changes in the flow patterns in the bed may be projected.

The aim of this paper is to use this approach to quantify the effect of flowrate changes on liquid distribution in representative drip irrigated heap leaching systems, applying the

techniques developed in Fagan et al. (2013). Two aspects are considered: the liquid flow in a leaching column at steady state and the transient liquid distribution in the immediate vicinity of the drip irrigation point source using a setup with a greater ore bed breadth. The desired application is to ascertain if a change in flowrate can be used to manipulate liquid flow in a packed bed in order to facilitate improved liquid distribution and hence contacting of the leaching solution with the ore.

## 2 MATERIALS AND METHODS

### 2.1 Ore

A low grade copper ore (average composition 2.95% Fe, 0.69% Cu and 2.02% S by weight) which had a particle size distribution as detailed in Table 1 was used in the experiments. The average internal porosity of the ore was 4.6%. The ore was agglomerated with 0.1 M sulfuric acid using a liquid to ore ratio of 5 mL per 100 g.

**Table 1.** Particle size distribution for the ore used in the leaching column.

| Size (mm) | Weight (%) |
|---|---|
| 25.4 – 13.2 | 13.9 |
| 13.2 – 9.5 | 18.4 |
| 9.5 – 5.6 | 20.3 |
| 5.6 – 2.0 | 19.8 |
| 2.0 – 0.71 | 9.1 |
| < 0.71 | 18.5 |

### 2.2 Column leaching experiment

#### 2.2.1 Preparation and operation

A sample of agglomerated ore (600 g) was packed into the glass column shown schematically in Figure 1, the inner diameter of which was restricted to 50 mm by the spectrometer's internal bore. The gravimetric voidage of the packed ore was determined to be 38.0±0.8% by

flooding the column from the base upwards following construction of the bed, after which the column was drained. The bed was irrigated drip-wise using a peristaltic pump at flowrates of 10, 20 and 40 mL $h^{-1}$, approximately equivalent to 5, 10 and 20 L $m^{-2}$ $h^{-1}$. The liquid feed was water that had been doped with 0.8 g $L^{-1}$ of $GdCl_3 \cdot 6H_2O$ in order to shorten the MRI acquisition time. The system was considered to have reached steady state at each flowrate when the outlet and inlet flows matched. A minimum of 12 hours was allowed once the bed had achieved this condition before any MRI experiments were conducted. The liquid hold-up was determined gravimetrically at the steady state condition for each flow rate by performing a balance on the liquid based on the approach of Bouffard and Dixon (2001). This accounted for the agglomeration liquid, the liquid that had been added to the column (during flooding and subsequent irrigation) and the liquid that had been drained from the column (drainage following flooding and subsequent drainage during normal unsaturated irrigation). Following acquisition of all desired data at a given flowrate, the flowrate was stepped up to the next highest rate without any disruption in the flow and steady state allowed to re-establish.

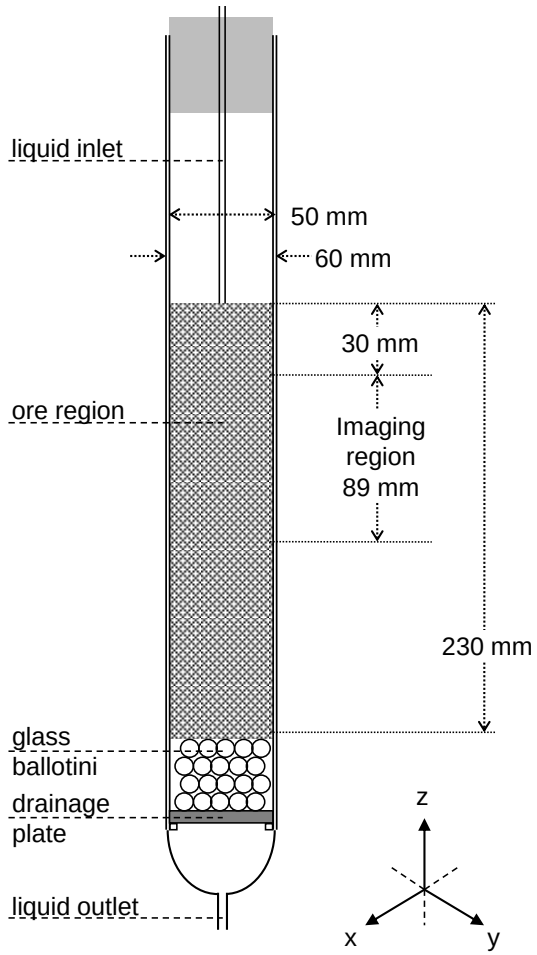


**Figure 1.** Schematic of the leaching column with the ore bed and imaging region heights indicated.

### 2.2.2 Magnetic resonance imaging

The column imaging was performed on a Bruker AV III 300, 7.1 T vertical bore spectrometer with a wide bore radio frequency (RF) coil which had an inner diameter of 66 mm. The field of view (FOV) was approximately 53 mm × 53 mm in the x and y directions and 89 mm in the z (vertical) direction. The z (along the bore height) FOV was longer than the length of the homogeneous imaging region of the coil to prevent wrap-around artefacts. The 3D acquisition size was 64×64×64 which corresponds to a nominal resolution of 830 μm per pixel in the x and y directions and 1390 μm in the z direction. A standard SESPI acquisition

sequence was used as is described in Fagan et al. (2012). It utilised a total gradient encoding time ($t_p$) of 300 μs, a repeat time (*TR*) of 50 ms and an echo time (*TE*) of 750 μs. Four repeat scans were done for phase cycling and eight points were acquired along each echo at 5 μs intervals for signal averaging to improve the signal to noise ratio (SNR).

### 2.2.3 MRI image analysis

#### 2.2.3.1 Phase mapping

The distributions of the different phases (gas, liquid and solid) in the column were mapped and analysed using the methodology developed by Fagan et al. (2013). This required the acquisition of images of the unsaturated flowing column at the different flowrates as well as a 3D image of the flooded column. The latter acquisition was necessary to identify the total void space available in the ore bed. The flooded column images were acquired at the start of the experiment at the same time as the gravimetric voidage measurement.

The 3D images were thresholded in MATLAB® using a histogram analysis of the signal, thereby removing noise. The thresholding converted the images into a binary format which identifies the voxels that contain liquid and those which do not. The binary flowing images were combined with that of the flooded column to produce phase maps which show the gas, liquid and solid positions within the column. A detailed description of this procedure, how partial volume elements are accounted for in it and hence its accuracy may be found in Fagan et al. (2013).

The spatial distributions of the pore space and of the liquid relative to the solid ore were quantified using the phase maps. These were calculated using the pore thinning algorithm of Baldwin et al. (1996) on the total void space after which the liquid pixels were identified, as

detailed in the methods paper by Fagan et al. (2013). The liquid – solid and liquid – gas interfacial areas were also quantified from the phase maps. The interfacial area measurements excluded the pixels adjacent to the column walls to avoid including wall effects.

#### 2.2.3.2 Signal magnitude

Analysis based on the signal magnitudes of the pixels in the MRI acquisitions used the raw image data which had been filtered for noise, as per the phase map preparation (Section 2.2.3.1). As the SESPI echo time (750 μs) is much shorter than the $T_2$ of the doped water (longer than 20 ms in all the samples tested as measured using the standard CPMG pulse sequence) it may be concluded that the signal magnitude is a quantitative measure of the amount of liquid present for the ore systems.

## 2.3 Horizontal cell experiment

### 2.3.1 Preparation and operation

In the second experimental setup the ore was packed into the tubular horizontal Perspex cell depicted in Figure 2. Two samples were tested to assess repeatability. For each run, 1 kg of agglomerated ore was packed into the bed such that the height of the packing region was 47 mm and the length of the bed was 170 mm. A layer of 10 mm glass ballotini was placed below the ore on a drainage plate (3 mm aperture grid). This setup prevented the loss of fines from the ore bed and created a liquid disengagement region at the cell base, thereby avoiding undesirable upwards wicking of the liquid (confirmed using the MRI acquisitions). Ready drainage of the liquid from the cell was achieved through a 5 mm outlet port at the side of the base.

The ore was drip-irrigated with 0.8 g $L^{-1}$ $GdCl_3 \cdot 6H_2O$ doped water as before. This was done from a single point, located at the top and centre of the cell, thereby minimising wall effects on the liquid flow. Flowrates of 10, 20 and 40 mL $h^{-1}$ were used, approximately equivalent to between 1 and 5 L $m^{-2}$ $h^{-1}$. In addition to acquiring images at steady state as was done for the column experiments, it was desired to track the initial wetting of the bed (i.e. during unsteady state flow). The sample was therefore dried overnight in an oven at 70°C to ensure that there was no signal from liquid in the sample at the start of each experiment. The ore beds were deemed to have reached steady state liquid flow when the inlet and outlet flows for the system had matched for at least 12 hours.

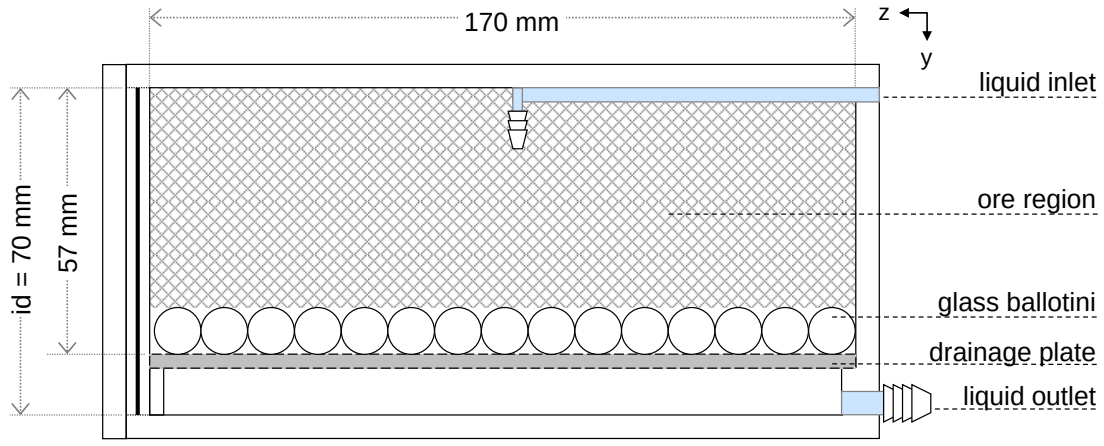


**Figure 2.** Illustration of the tubular horizontal cell used to examine the effect of flowrate changes around a single drip irrigation point.

### 2.3.2 Magnetic resonance imaging

Imaging of the horizontal cell was performed on a Bruker AV 85, 2 T horizontal bore spectrometer equipped with a wide bore RF coil which had an inner diameter of 83 mm. The FOV was 80 mm × 80 mm in the x and y directions and 160 mm in the z (along the bore length), which is again longer than the length of the homogeneous imaging region of the coil

(closer to 100 mm) to prevent wrap-around artefacts. The 3D acquisition size was 32×32×64 which corresponds to a nominal resolution of 2.5 mm per pixel in all three directions. The SESPI acquisition sequence and imaging parameters were the same as for the column experiment (Section 2.2.2).

The 2D projections (x-y and y-z) were acquired of the setup before irrigation was started to confirm that the sample was dry and to have a background signal map. The projections were also used to position the cell correctly within the spectrometer bore, with signal from a small piece of Blu-Tack® above the elbow connector enabling accurate positioning. The 2D projections were acquired at 4, 15, 30 and 60 minutes intervals once irrigation had started, followed by hourly scans until a steady state was observed at which point a 3D image was acquired.

### 2.3.3 MRI image analysis

#### 2.3.3.1 Thresholding

All images were thresholded at a common level in MATLAB® using a histogram analysis of the signal for noise to be removed. The binary images that resulted were then used to assess the percentage of the imaging region that contained liquid.

#### 2.3.3.2 Signal magnitude profiles

Signal magnitude profiles were generated along the length (z) of the cell by summing the signal in the x and y directions in the 3D steady state acquisitions. Because the liquid signal relaxation time of the samples tested (>20 ms) was much longer than the imaging method echo time (750 μs), these signal magnitude profiles are equivalent to liquid hold-up profiles,

as MRI pixel signal magnitude is directly proportional to the amount of liquid present in that location (Fagan et al., 2012).

## 3 RESULTS AND DISCUSSION

### 3.1 Column leaching experiment

#### 3.1.1 Liquid hold-up

Figure 3 shows an example of equivalent 2D slices (extracted from the 3D data) of the column flooded and at the different flowrates along with the corresponding thresholded images. The phase map calculated voidage of 37.9±3.9%, where the error range indicates the variation within the column, agrees with the gravimetrically determined voidage of 38.0±0.8% thereby confirming the validity of the thresholding level.

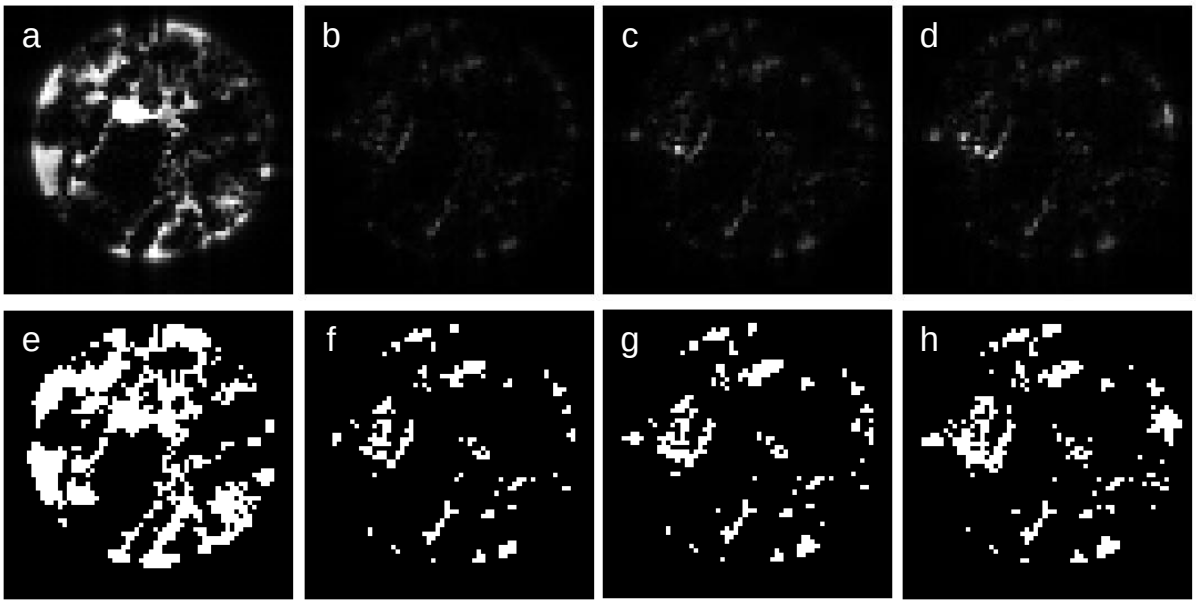


**Figure 3.** 2D slices extracted from the 3D acquisitions of the column (a) flooded and flowing at (b) 10, (c) 20 and (d) 40 mL $h^{-1}$. The corresponding thresholded images are shown directly below in figures (e) to (h).

The changes in the percentage liquid hold-up of the column under the different flowing conditions were calculated using three approaches:

a) Gravimetric measurement based on a liquid balance
b) By quantifying the liquid filled volume in the phase maps
c) By considering the total (summed) signal magnitude in the flowing MRI acquisitions

The second MRI technique (c) does not require the application of a thresholding level and the increase in signal should be directly proportional to the amount of liquid present, both internal and external to the ore. This follows because SESPI acquisitions of ore systems have been demonstrated to have only minor $T_2$ weighting (Fagan et al., 2012). The inclusion of method (c) is necessary to confirm that low signal magnitude pixels which are representative of internal liquid content or thin liquid films are not being incorrectly excluded in method (b). Note that the gravimetric measurement was necessarily done for the whole sample, whereas the MRI quantification methods only considered the imaging region. The results of all of the methods are given in Table 2.

The two MRI liquid quantification methods produce similar relative increases in the liquid hold-up. This confirms that the phase map method for the liquid hold-up quantification gives an acceptable value for the amount of liquid in the bed and is not unduly biased towards larger liquid volumes. The phase map values also compare favourably with the traditional gravimetric measurements. Each doubling of the flowrate results in a small absolute increase in the liquid hold-up of between 2% and 3%. The increase in the percentage liquid hold-up when the flowrate increases from 10 to 20 mL $h^{-1}$ was marginally higher than for the subsequent increase to 40 mL $h^{-1}$. This is in line with literature (Bouffard and Dixon, 2001; Ilankoon and Neethling, 2012).

**Table 2.** Change and relative increase in percentage liquid hold-up of the ore bed as a function of flowrate determined using different methods*.

| | a) Gravimetric | | b) Phase map | | c) MRI signal | |
|---|---|---|---|---|---|---|
| Flowrate (mL $h^{-1}$) | Hold-up (%) | Relative increase (%) | Hold-up (%) | Relative increase (%) | Signal (a.u.) | Relative increase (%) |
| 10 | 13.6 ± 1.8 | - | 12.8 ± 3.2 | - | 1.0 | - |
| 20 | 17.1 ± 3.4 | 26% | 15.8 ± 3.3 | 23% | 1.2 | 19% |
| 40 | 19.2 ± 0.9 | 12% | 18.4 ± 3.2 | 16% | 1.4 | 14% |

*(a) Gravimetric measurement, (b) quantification from phase maps, (c) comparison to total MRI signal

The signal magnitude of a pixel in MRI acquisitions is proportional to the amount of liquid held in that region, given the absence of influence by spatially variable signal relaxation times. Therefore the highest intensity pixels indicate the position of larger volumes of liquid, likely channels, where the pixel is liquid filled. Pixels of lower signal magnitude are indicative of liquid held by capillary forces in small pores or in thin films, unless they fall on the edge of larger channels.

Figure 4 shows that there was an increase in the amount of liquid in all of the pixel magnitude ranges (Figure 4a), but that the fraction of the total liquid volume held in high magnitude pixels increased while the fraction held in the lowest magnitude pixels decreased (Figure 4b). This suggests that as the flowrate increased the fraction of the liquid that flowed in channels increased relative to the liquid volume retained by capillary action in pores. This agrees with Bouffard and Dixon (2001) whose gravimetric experiments showed that the flowing liquid hold-up increases with increasing flowrate while the stagnant liquid hold-up remains roughly unchanged. This follows because the capillary suction held liquid volume is determined by the local porosities. The additional liquid would rather have passed through the bed via newly established preferential paths. The absolute increase in the lower signal magnitude pixels

with flowrate (Figure 4a) however may indicate that more channel flow resulted in an increase in liquid-ore contacting thereby contributing to some increase in capillary held liquid.

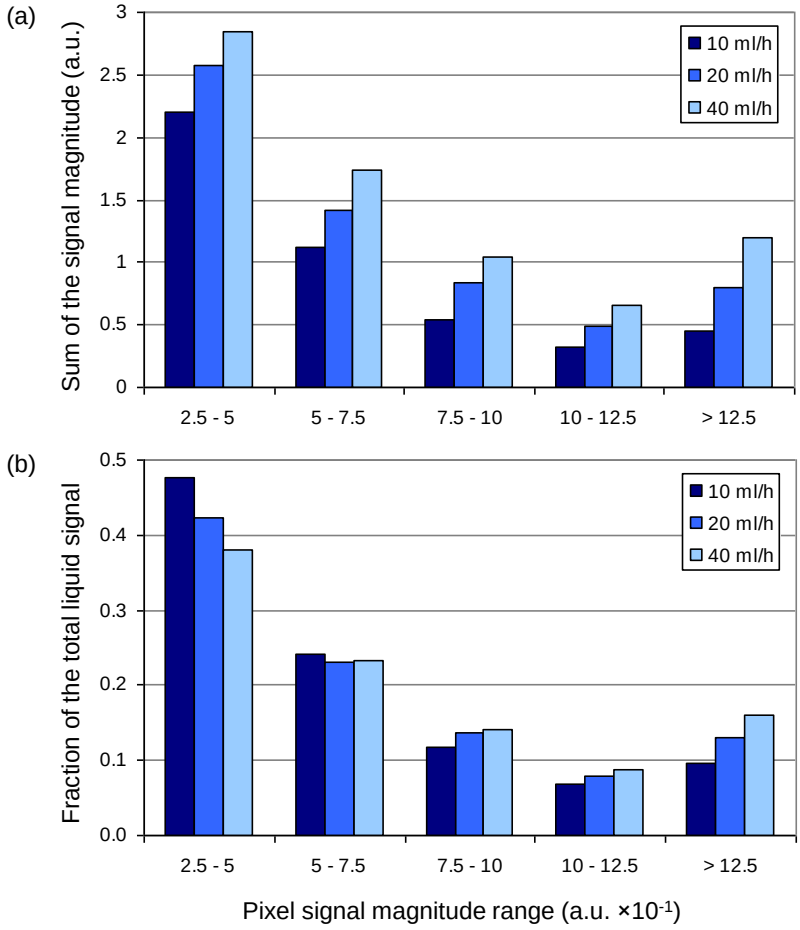


**Figure 4.** Distribution of the liquid signal at different flowrates where the signal magnitude is proportional to the volumetric liquid content of the pixel, presented as (a) the sum of the signal magnitude in each range and (b) the fractional contribution of that signal to the overall total.

### 3.1.2 Spatial distribution of the liquid

The MRI results have the advantage of allowing for the spatial resolution of the liquid hold-up, which gravimetric measurements do not. The positions of the liquid and pore space relative to the ore surface are presented in Table 3 and the percentages of the different regions of the pore space occupied by liquid are presented in Table 4.

Three quarters or more of the liquid was located within less than 1 mm of the ore surface and more than 99% of the liquid was within 2 mm. Furthermore, the percentage of the pore space that was liquid filled decreased as the distance from the ore surface increased. This indicates that there was a stronger preference for surface flow in this ore packing than there was in the MRI study presented by Fagan et al. (2013) which was conducted using the same column setup and ore type, irrigated at 40 mL $h^{-1}$. In that study less than 60% of the liquid was less than 1 mm from the solid and more than 15% was located further than 2 mm from the ore surface. The relatively smaller pore space in this ore bed, where 97% of the pore space is within 2 mm of the ore surface, means that a similar liquid distribution is not possible. This demonstrates the significant degree of variability in the hydrodynamics between different packed ore beds that MRI generated phase maps can identify.

For each increase in flowrate, the liquid occupation of the pore space increased by circa 4% in the 0 - 1 mm and 1 - 2 mm distance ranges. However, the liquid found 1 - 2 mm from the solid surface accounted for a larger percentage of the total liquid hold-up as the flowrate was increased, whereas the proportion located less than 1 mm from the solid surface decreased. Relatively negligible change occurred in the pore space further from the solid surface; this is not unexpected as this pore space accounted for less than 3% of the total. The increase in the amount of liquid positioned further from the solid surface at higher flowrates implies that relatively thicker rivulets formed in the ore bed at higher flowrates. This is also reflected in

the slight increase in the average distance of the liquid from the solid as the flowrate increased. Of the additional liquid retained by the ore bed following the increase in flowrate, 92.5±8.2% was not in contact with the existing liquid hold-up (at the lower flowrate). Thus additional liquid hold-up following an increase in liquid flowrate was in the form of new rivulets rather than due to the growth of existing rivulets, supporting the results of Section 3.1.1. This also agrees with and confirms the conjecture of Ilankoon and Neethling (2012) whose gravimetric experiments and models of heap hydrodynamics indicated that additional liquid hold-up in faster flowrate situations was due to the formation of new rivulets.

**Table 3.** Position of the pore (total void) space and the liquid in the column as a function of flowrate expressed as its distance from the solid ore surface.*

| Distance from solid ore surface (mm) | Pore space (%) | Liquid pixels (%) | | |
|---|---|---|---|---|
| | | 10 mL $h^{-1}$ | 20 mL $h^{-1}$ | 40 mL $h^{-1}$ |
| < 1 | 64.7 ± 0.5 | 78.2 ± 5.4 | 76.2 ± 6.5 | 74.2 ± 7.4 |
| 1 - 2 | 33.1 ± 0.7 | 21.7 ± 5.3 | 23.5 ± 6.5 | 25.5 ± 7.2 |
| 2 - 3 | 2.2 ± 0.2 | 0.2 ± 0.1 | 0.2 ± 0.1 | 0.3 ± 0.2 |
| 3 - 4 | 0.1 ± 0.0 | 0.0 | 0.0 | 0.0 |
| > 4 | 0.02 ± 0.00 | 0.0 | 0.0 | 0.0 |
| Average distance (mm) | 1.06 ± 0.38 | 0.95 ± 0.25 | 0.96 ± 0.26 | 0.97 ± 0.27 |
| Max distance (mm) | 4.68 | 2.90 | 2.90 | 2.90 |

*Error measurements were generated by considering partial volume effects.

**Table 4.** Percentage of the pore space occupied by the liquid as a function of the flowrate.*

| Distance from solid ore surface (mm) | Pore space occupied by liquid (%) | | |
|---|---|---|---|
| | 10 mL $h^{-1}$ | 20 mL $h^{-1}$ | 40 mL $h^{-1}$ |
| < 1 | 25.4 ± 10.3 | 30.1 ± 11.2 | 34.0 ± 12.3 |
| 1 - 2 | 14.7 ± 9.5 | 19.0 ± 12.1 | 24.0 ± 15.6 |
| 2 - 3 | 2.0 ± 1.6 | 3.3 ± 2.6 | 4.4 ± 4.3 |
| 3 - 4 | 0.0 | 0.0 | 0.0 |
| > 4 | 0.0 | 0.0 | 0.0 |

*Error measurements were generated by considering partial volume effects.

### 3.1.3 Interfacial areas

The effect of changing the flowrate on the interfacial areas between the three phases is illustrated in Figure 5. The liquid-solid interfacial area increased as the liquid flowrate was increased. This is in line with the formation of new rivulets along the ore surface. Therefore increasing the flowrate has the advantage of increasing the amount of liquid-solid contact in a column experiment which has the potential to improve leaching efficiencies as more of the mineral in the ore will come into contact with the leaching solution. By contrast, the gas-liquid interfacial area decreased as the flowrate was increased. This is explained by an increase in the rivulet thickness at the higher flowrates. The decrease will have the effect of increasing the diffusion path for oxygen and carbon dioxide from the gas through the liquid to the reaction sites and any bioleaching microorganisms. This may negatively impact mineral recovery since the liquid mass transfer of oxygen is proposed to be one of the key rate limiting processes (Petersen, 2010a, 2010b). Another possible contributor to the decrease in interfacial area is a greater confluence of rivulets at the higher flowrates. It is likely that an optimal flowrate exists that balances the effect of the liquid-solid and gas-liquid contact areas, though the leaching experiments to determine this point were not considered as part of this study.

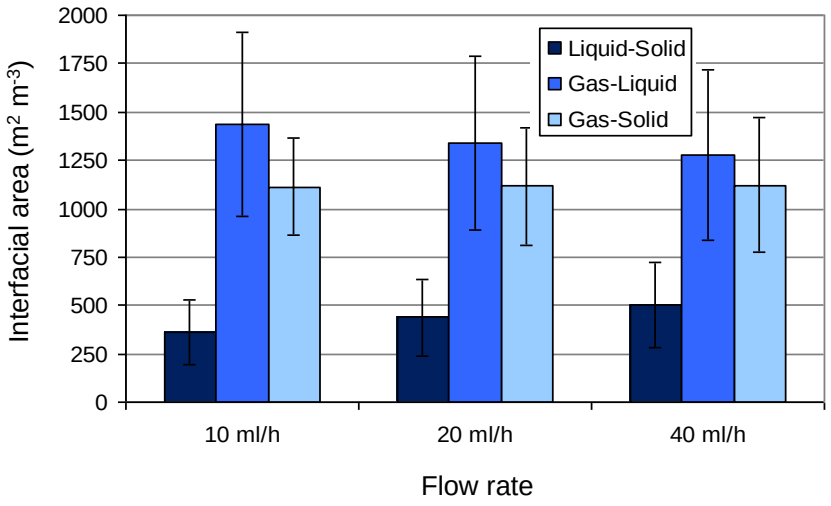


**Figure 5.** Interfacial areas between the gas, liquid and solid phases as a function of flowrate. The error bars indicate the maximum and minimum interfacial areas when partial volume effects are considered.

### 3.2 Horizontal cell experiments

The small diameter of the column used for Section 3.1 meant that variations across the column diameter were not observable. The second setup where the packed ore width was 170 mm along the horizontal bore length was consequently used to enable the liquid distribution from a single drip emission point to be examined and for the effect of flowrate thereon to be quantified.

#### 3.2.1 Overall liquid occupation

The 2D y-z projections acquired of the two horizontal cell (Figure 2) samples irrigated at the three flowrates are presented in Figure 6 and Figure 7. Table 5 summarises the percentage of the imaging region that contained liquid at the corresponding different irrigation volumes, calculated from the thresholded images.

Liquid breakthrough at the base of the ore bed occurred faster at the higher irrigation rates which is indicative of a bias towards gravitation dominated flow (Ilankoon and Neethling, 2014). A broad wetting front was evident at all flowrates, an effect of lateral movement of the liquid under capillary suction. Initially, when only 10 mL of liquid had been irrigated, the liquid occupied region in the first sample increased with flowrate. This trend did not occur in the second sample, where the least extensive wetting was in the 20 mL $h^{-1}$ run. The liquid occupied region then decreased with increasing flowrate for both samples when 20 and 40 mL had been irrigated. This is because the liquid did not extend as far laterally from the irrigation point at the higher flowrates which indicates that there was less influence due to capillary suction at the higher flowrates. This effect has previously been discussed by O'Kane Consultants Inc. (2000) and is the cause of macro-pore preferential flow. The measurements at the 10 mL stage may have deviated from this trend because the liquid flow was not yet sufficiently established. The liquid occupied region was larger in the second sample than in the first sample for all irrigation volumes and flowrates. This may be attributed to variations in the structure of the agglomerated ore bed and the relative location of the fine and large ore particles in the two samples.

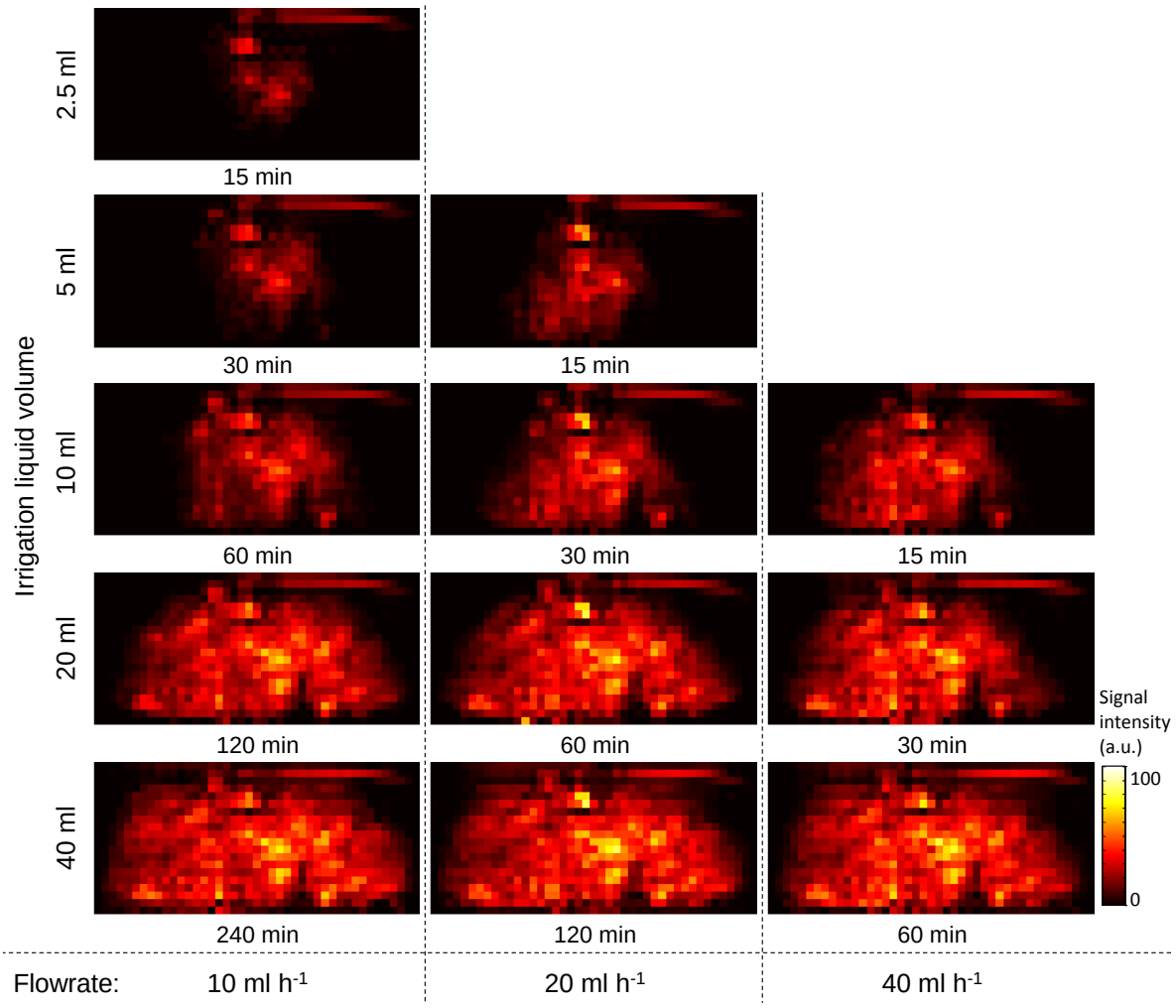


Figure 6. Comparison of the liquid distribution in the first agglomerated ore sample for different flowrates after the same volume of liquid has been introduced to the system.

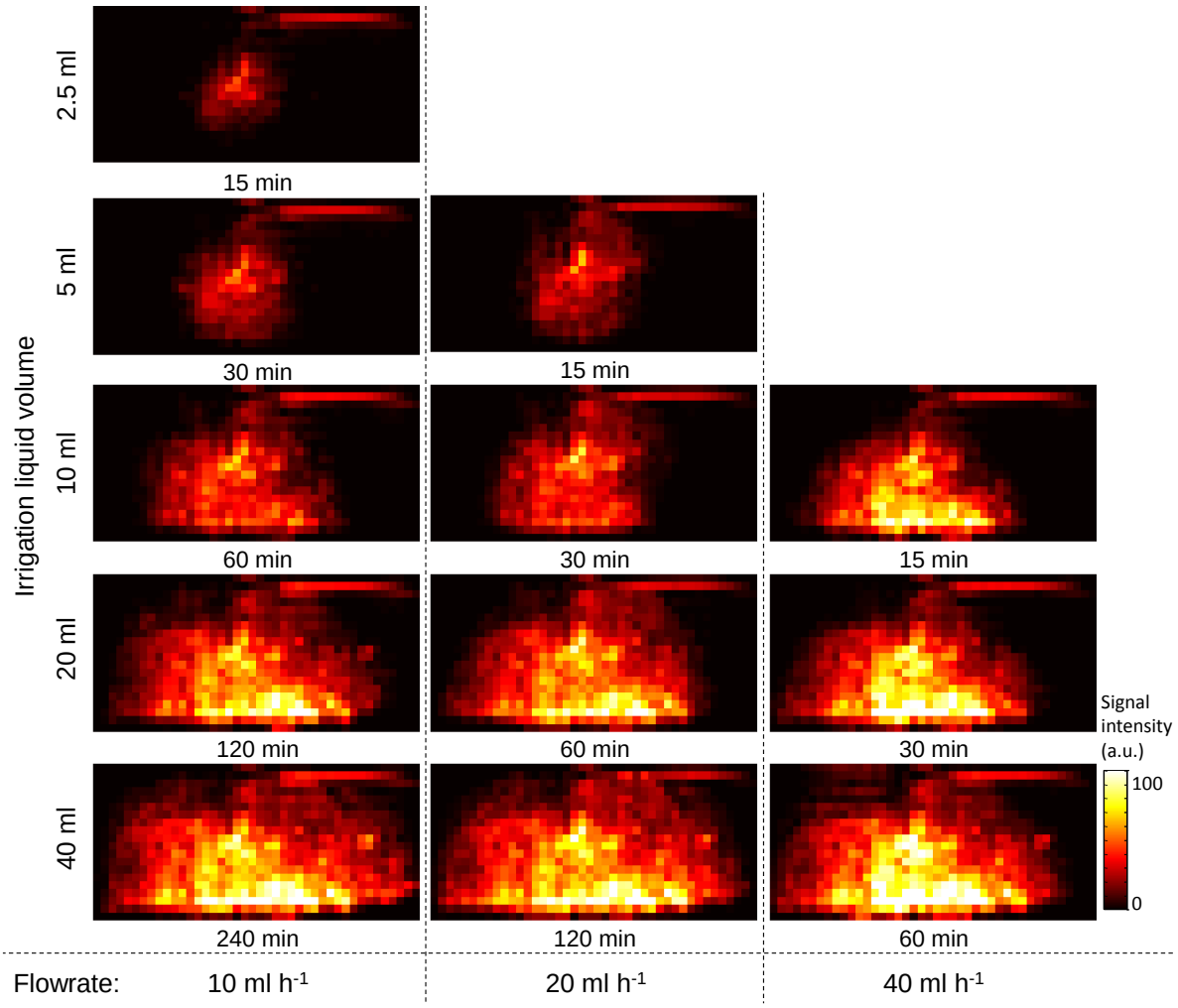


Figure 7. Comparison of the liquid distribution in the second agglomerated ore sample for different flow rates after the same volume of liquid has been introduced to the system.

Table 5. Imaging region in the y-z projections of the agglomerated ore occupied by liquid.

| Volume of irrigated liquid (mL) | Sample 1 liquid occupied area (%) | | | Sample 2 liquid occupied area (%) | | |
|---|---|---|---|---|---|---|
| | 10 mL $h^{-1}$ | 20 mL $h^{-1}$ | 40 mL $h^{-1}$ | 10 mL $h^{-1}$ | 20 mL $h^{-1}$ | 40 mL $h^{-1}$ |
| 10 | 30.6 | 33.8 | 37.0 | 44.4 | 42.4 | 45.7 |
| 20 | 64.9 | 64.0 | 56.9 | 67.6 | 66.6 | 60.7 |
| 40 | 76.9 | 75.6 | 74.5 | 86.2 | 84.7 | 77.2 |

### 3.2.2 Horizontal variations in hold-up

Signal magnitude profiles are presented in Figure 8 which show how the local liquid hold-up varied as a function of distance from the irrigation point at steady state. The dips in the profiles (particularly evident in sample 1) are due to the existence of large ore particles in these locations.

In the first sample, the change in the overall signal magnitude indicated that the relative increase in hold-up increased by 6% with the initial flowrate doubling and subsequently by 1% with the second doubling. The hold-up increased by 6% and 7%, respectively, in the second sample. These relative increases are much less than was observed in the column experiments (Table 2). The profiles show that the amount of liquid retained by the ore bed decreased as the distance from the irrigation point increased. This is because more of the liquid in the outer regions will have moved there under capillary suction and the retention will consequently be a function of the local ore particle sizes rather than the flowrate of the liquid. Furthermore, as the distance from the irrigation point increased, the differences in the liquid retention at different flowrates decreased. In the centre of the ore bed a higher flowrate clearly resulted in an increase in the liquid hold-up, with only a few local exceptions in sample 1. In contrast to this, in some regions of the samples (more than 20 mm to the left and 15 mm to the right of the irrigation point in sample 1 and more than 17.5 mm to the right of the irrigation point in sample 2) there was almost no change in the liquid retention for all of the flowrates. Note that these distances correspond closely to the radius of the column (25 mm) used in Section 3.1 which confirms why similar behaviour was not observed then.

This indicates that though liquid hold-up increases slightly with flowrate, the effect decreases as the distance from the irrigation point increases which agrees with the predictions of Dixon

(2003). Their model of the solution flow in a heap from a single point source, based on the solution of the Richards' equation, indicated that not much lateral liquid flow occurs away from the channels of flow after the initial wetting of the ore and that the majority of flow is limited to within a few centimetres of the vertical axis (the irrigation point) despite a significant degree of saturation being achieved throughout the entire ore bed. Therefore changing the liquid flowrate was not found to be an effective method for perturbing the liquid flow paths beyond the region below the drip irrigation point.

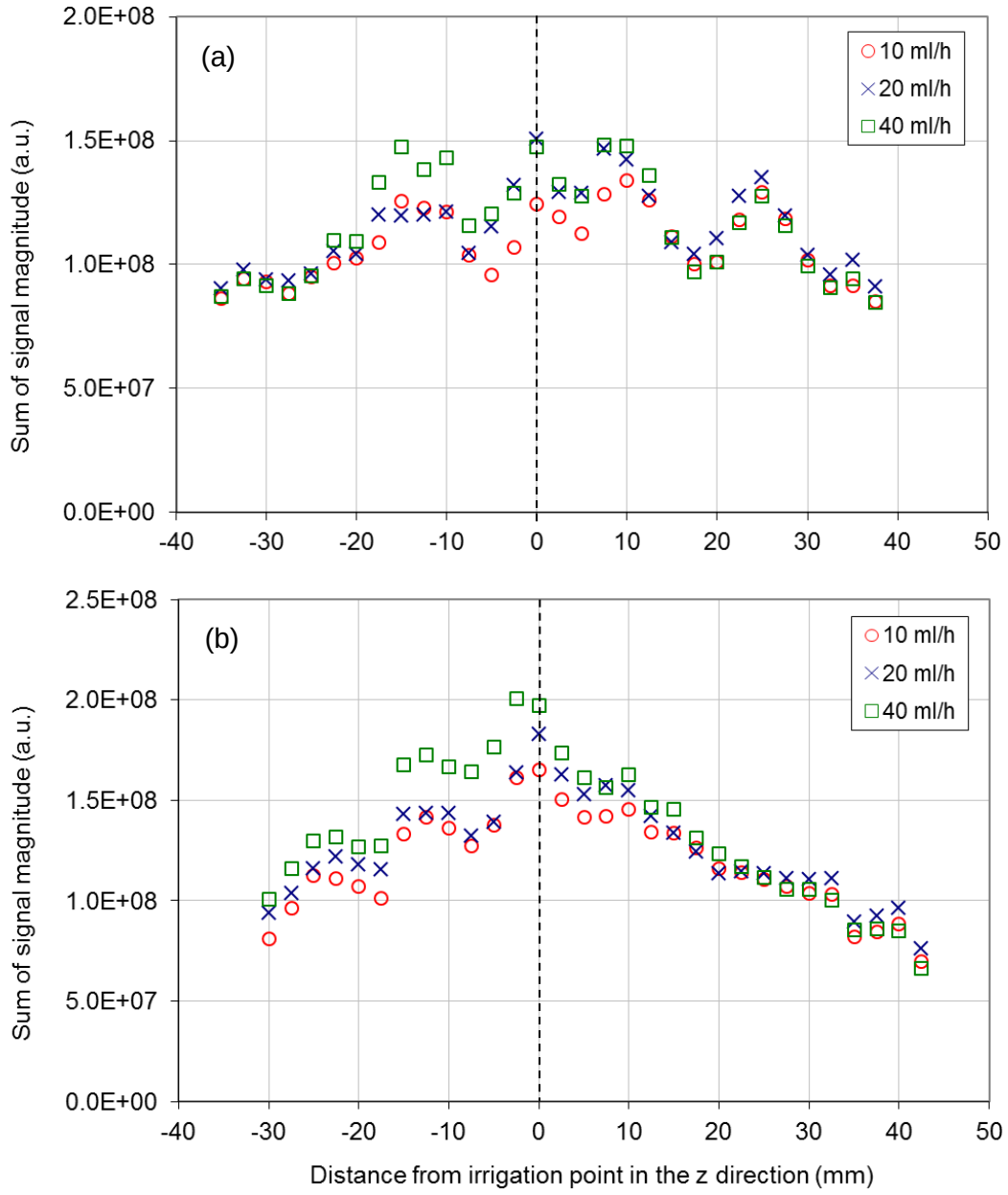


Figure 8. The steady state signal magnitude profiles for the three flowrates applied to the (a) first and (b) second ore samples, where signal is equivalent to local liquid hold-up.

# 4 CONCLUSIONS

The experiments have demonstrated that MRI acquisitions can successfully be used to discern changes in liquid distribution in unsaturated ore beds that result from irrigation flowrate changes.

The 3D acquisitions of an unsaturated column showed that an increase in flowrate caused the liquid hold-up to increase as expected. The images indicated that this was due to the formation of new rivulets in the ore bed, accompanied by an overall increase in the average thickness of the liquid films. This improved the measured liquid-solid interfacial area, an advantageous result as more of the mineral in the ore is potentially contacted with the leaching solution.

In the experiments with an ore bed of larger breadth, doubling of the flowrate resulted in comparatively small increases in the liquid hold-up, limited to the region directly below and adjacent to the drip irrigation point. This was attributed to the fact that the main effect of the higher liquid flowrate was to increase the amount of liquid held in channels (macro-pore flow). The flow of this liquid is gravitationally dominated, and hence its influence limited to the region below the irrigation point. The capillary held liquid away from these main channels appeared unchanged. Hence the regions that received improved wetting with the increase in flowrate were the same regions that were well wetted initially.

Therefore, while the change in flowrate influences the liquid distribution for this ore packing, the fact that the effect was limited to macro-pore gravitational flow means that flowrate increments were unsuccessful at perturbing the liquid distribution in a way that would be beneficial to the recovery of previously poorly wetted mineral in the majority of a heap

volume. This prompts the need for investigating other techniques for flow perturbation for improved leaching recoveries, for example ripping of the heap surface to promote the establishment of new preferential flow paths.

## ACKNOWLEDGEMENTS

The authors would like to acknowledge and thank the University of Cape Town, BHP Billiton, the Cambridge Commonwealth Trust and Trinity College Cambridge for their sponsorship and support of this project.

## REFERENCES

Baldwin, C.A., Sederman, A.J., Mantle, M.D., Alexander, P., Gladden, L.F., 1996. Determination and characterization of the structure of a pore space from 3D volume images. J. Colloid Interface Sci., 181(1): 79–92.

Bartlett, R.W., 1998. Solution Mining: Leaching and Fluid Recovery of Materials, second ed. Gordon and Breach Science Publishers.

Bouffard, S.C. and Dixon, D.G., 2001. Investigative study into the hydrodynamics of heap leaching processes. Metall. Mater. Trans. B, 32(5): 763–776.

Bouffard, S.C. and West-Sells, P.G., 2009. Hydrodynamic behavior of heap leach piles: Influence of testing scale and material properties. Hydrometallurgy, 98(1-2): 136–142.

Chiume, R., Minnaar, S.H., Ngoma, I.E., Bryan, C.G. and Harrison, S.T.L., 2012. Microbial colonisation in heaps for mineral bioleaching and the influence of irrigation rate. Miner. Eng., 39: 156–164.

De Andrade Lima, L.R.P., 2006. Liquid axial dispersion and holdup in column leaching. Miner. Eng., 19: 37–47.

Decker, D.L. and Tyler, S.W., 1999. Hydrodynamics and solute transport in heap leach mining. In: D. Kosich and G. Miller (Eds.), Closure, Remediation & Management of Precious Metals Heap Leach Facilities.

Dixon, D.G., 2003. Heap leach modeling – the current state of the art. In: C.A. Young et al. (Eds.), H*ydrometallurgy 2003, Volume 1: Leaching and Solution Percolation*. The Minerals, Metals and Materials Society, Warrendale, Pennsylvania, pp. 289–314.

Fagan, M.A., Sederman, A.J., Harrison, S.T.L. and Johns, M.L., 2013. Phase distribution identification in the column leaching of low grade ores using MRI. Miner. Eng., 48: 94–99.

Fagan, M.A., Sederman, A.J. and Johns, M.L., 2012. MR imaging of ore for heap bioleaching studies using pure phase encode acquisition methods. J. Magn. Reson., 216: 121–127.

Guzman, A. Scheffel, R.E., Flaherty, S.M., 2006, Geochemical Profiling Of A Sulfide Leaching Operation: A Case Study. SME Annual Meeting 2006, St. Louis.

Ilankoon, I.M.S.K. and Neethling, S.J., 2012. Hysteresis in unsaturated flow in packed beds and heaps. Miner. Eng., 35: 1–8.

Ilankoon, I.M.S.K. and Neethling, S.J., 2014. Transient liquid holdup and drainage variations in gravity dominated non-porous and porous packed beds. Chem. Eng. Sci. 116: 398–405.

O'Kane Consultants Inc., 2000. Demonstration of the application of unsaturated zone hydrology for heap leaching optimization. Industrial Research Assistance Program Contract # 332407(628-1).

Petersen, J., 2010a. Determination of oxygen gas-liquid mass transfer rates in heap bioleach reactors. Miner. Eng., 23(6): 504–510.

Petersen, J., 2010b. Modelling of bioleach processes: Connection between science and engineering. Hydrometallurgy, 104(3-4): 404–409.

Petersen, J. and Dixon, D.G., 2007. Modeling and optimization of heap bioleach processes. In: D.E. Rawlings and B.D. Johnson (Eds.), Biomining. Springer-Verlag, pp. 153–176.

van Hille, R.P., van Zyl, A.W., Spurr, N.R.L., and Harrison S.T.L., 2010, Investigating heap bioleaching: Effect of feed iron concentration on bioleaching performance. Miner. Eng., 23: 518–525.

Wu, A.X., Yin, S.H., Yang, B.H., Wang, J. and Qiu, G.Z., 2007. Study on preferential flow in dump leaching of low-grade ores. Hydrometallurgy, 87(3-4): 124–132.